Scripta Materialia 196 (2021) 113760

Contents lists available at ScienceDirect

Scripta Materialia

journal homepage: www.elsevier.com/locate/scriptamat

High-coercivity $ThMn_{12}$-type monocrystalline Sm–Zr–Fe–Co–Ti particles by high-temperature reduction diffusion

A.M. Gabay*, G.C. Hadjipanayis

Department of Physics and Astronomy, University of Delaware, 217 Sharp Lab, Newark, DE 19716, USA

ARTICLE INFO

Article history:
Received 5 January 2021
Revised 21 January 2021
Accepted 22 January 2021
Available online 4 February 2021

Keywords:
Mechanochemical synthesis
Powder processing
Rare earth magnets
Magnetic anisotropy
Coercivity

ABSTRACT

The $ThMn_{12}$-type $(Sm,Zr)_1(Fe,Co,Ti)_{12}$ compounds have the potential of powerful permanent magnets. Magnetically hard and anisotropic powders of such compound have been prepared by subjecting elemental oxides and Co mixed with Ca and CaO dispersant to a succession of high-energy ball-milling, reduction diffusion at 990–1220°C and repeated washing. The size of the resulting $ThMn_{12}$-type crystallites, their coercivity and fraction of monocrystalline particles were all found to increase with the reduction-diffusion temperature. Particles synthesized at 1220°C were highly monocrystalline with a mean size of 0.54 μm and, after a magnetic-field alignment, exhibited a coercivity of 1.26 T and a full-density-projected maximum energy product of at least 209 kJ/m^3 (26.3 MGOe). The strong positive effect of the reduction-diffusion temperature on the coercivity has been attributed to separation of the crystallites and to decrease in the incidence of structural defects.

To effectively utilize the excellent intrinsic magnetic properties of the $ThMn_{12}$-type compounds (the "1:12" compounds) represented by the formula $Sm_{1-x}Zr_x(Fe,Co)_{12-y}Ti_y$ [1–3], the future permanent magnets must be *textured* with the *c*-axes of individual crystallites lying in the same direction. The weak effect of hot plastic deformation on orientation of the $Sm(Fe,M)_{12}$ crystallites [4] and the absence of obvious conditions for an effective magnetic-field annealing leave preparation of *anisotropic powders* as the most realistic pathway for the creation of such texture. Conveniently enough, pulverization is also a powerful technique for the development of the intrinsic coercivity $\mu_0 H_c$. So far, however, attempts to pulverize the $Sm_{1-x}Zr_x(Fe,Co)_{12-y}Ti_y$ alloys with cutter mill [5], jet mill [6] and hydrogen treatment [7], as well as an attempt to synthesize the anisotropic powder via the reduction diffusion at 950°C [8] could only produce materials with $\mu_0 H_c \leq 0.15$ T. Although disappointing, these low $\mu_0 H_c$ values are not particularly surprising; even in the case of *nanocrystalline* $Sm_{1-x}Zr_x(Fe,Co)_{12-y}Ti_y$ alloys, the $\mu_0 H_c$ values were reported to reach 0.5–0.6 T at the most [9–12]. Easy nucleation of a reversed magnetization at the boundaries between the 1:12 crystallites [13] or at the twin boundaries with in the 1:12 crystallites [14] are believed to be responsible for this underperformance. Data reported in this letter demonstrate that reduction diffusion at ≈1200°C does produce 1:12 particles of a Sm–Zr–Fe–Co–Ti alloy exhibiting a very high $\mu_0 H_c$. This temperature is markedly higher not only than the 950°C recently used by Dirba et al. [8], but also than 1000°C and 1100°C explored in the earlier synthesis of, respectively, $Sm_{1-x}Ce_x(Fe,Co)_{11}Ti$ [15] and $Nd(Fe,Ti)_{12}$ [16]. Previously the authors already achieve a high $\mu_0 H_c$ of 1.08 T in a different, Si-stabilized 1:12 alloy which was reduced – after mechanical activation – at 1150°C [17], but they obtained a disappointingly low $\mu_0 H_c$ of 0.21 T in a $Sm_{0.9}Zr_{0.1}(Fe_{0.75}Co_{0.25})_{11.35}Ti_{0.65}$ alloy reduced at 1150°C [18].

Powders of Sm_2O_3 (217 mg), ZrO_2 (30 mg), Fe_2O_3 (599 mg), Co (101 mg) and TiO_2 (53 mg) were mixed with 956 mg of Ca (the reducing agent in the form of 1 mm granules) and 3 g of CaO (the dispersant prepared through in-house calcination of a submicron $CaCO_3$ powder). The mole ratios of the reactant elements, which can be presented as $Sm_{1.5}Zr_{0.3}(Fe_{0.81}Co_{0.19})_{11.19}Ti_{0.81}$ and $Ca_{1.6}O$, included large excesses of Sm and Ca. The mixed reactants and dispersant were milled for 4 h with six 12-mm steel balls in an argon-filled steel vial using a SPEX SamplePrep 8000 high-energy shaker mill. After this mechanical activation, 0.4–0.5 g of the resulting precursor powder was transferred under argon into a quartz capsule, where the precursor was separated from the quartz by an open-ended Mo-foil container. The capsule was sealed with 60 kPa of argon and placed in the tube furnace preheated to temperature of the reduction-diffusion annealing T_a; after 5 min, the capsule was taken out and allowed to cool down naturally. The annealing was followed by a nine-step washing to remove the reaction byproducts, leftover reagents and the dispersant; this process was described elsewhere [17] except that 2-

* Corresponding author.
E-mail address: gabay@udel.edu (A.M. Gabay).

https://doi.org/10.1016/j.scriptamat.2021.113760
1359-6462/

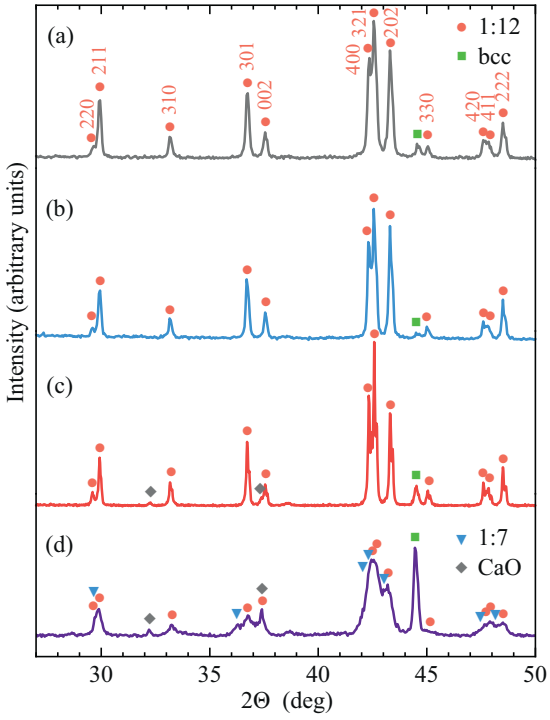

Fig. 1. XRD patterns of powders washed after reduction-diffusion synthesis at different T_a: (a) 990°C, (b) 1090°C, (c) 1220°C, (d) 1250°C. Crystal structures of the $ThMn_{12}$ type ("1:12"), $TbCu_7$ type ("1:7"), W type ("bcc") and NaCl type ("CaO") were identified.

propanol was used in the last two cycles instead of ethanol. Crystal structures of the products were studied with X-ray diffraction (XRD; a Rigaku Ultima IV instrument operating with the Cu K_α radiation) and analyzed with the Powder Cell software [19]. Morphology and composition of the products were determined with scanning electron microscopy (SEM) and energy-dispersive spectroscopy (EDS) using, respectively, a JEOL JSM-6335F microscope and a Zeiss Auriga 60 microscope equipped with an Oxford Instruments X-Max spectrometer. Magnetic characterization was done at 27°C with a Quantum Design VersaLab vibrating sample magnetometer. Powder particles were oriented with a 1.6 T magnetic field and immobilized with paraffin wax. Demagnetization curves were recorded after magnetizing the samples with a 10 T pulsed field. Self-demagnetization effects parallel and perpendicular to the magnetic-field alignment were corrected with demagnetization factors equal to 0.09 and 0.27, respectively; these factors had been determined by measuring similarly prepared Fe-powder samples.

Temperature of the reduction-diffusion annealing was varied from 990 to 1275°C; representative XRD patterns of the resulting alloys are shown in Fig. 1. The 1:12 structure with the lattice parameters $a = 0.8536(2)$ nm and $c = 0.4787(1)$ nm is the principal phase in the alloys prepared at 990°C $\leq T_a \leq$ 1220°C; a body-centered cubic (bcc) structure with $a = 0.2875(3)$ nm is the minority phase at 1.5–4.5 vol. %. Width of the 1:12 reflections decreases with the T_a, and eventually the reflections corresponding to the $K_{\alpha 1}$ and $K_{\alpha 2}$ wavelengths become separated (Fig. 1c). Such narrowing may manifest a number of different changes (better chemical homogeneity, larger crystallite size, reduced defects and strain of the lattice), but, in any case, the reflections recorded for the $T_a = 1220$°C clearly indicate a very high degree of the crystal order. When the T_a is increased to 1250°C, the phase composition changes dramatically: fraction of the bcc phase increases, the 1:12 reflections become broader, and a phase of the $TbCu_7$ type (the "1:7" phase) appears having very broad reflections with $a \approx 0.496$ nm, $c \approx 0.421$ nm. This change suggests that the upper temperature of the single-phase 1:12 region lies between 1220 and 1250°C. Because the annealed samples were not quenched, part of the 1:12 phase present in the alloy annealed at 1250°C might have actually formed during the cooling when the sample temperature decreased below 1220°C.

Area EDS characterization of the sample processed at 1090°C (the most pure 1:12 phase according to the XRD data) determined the following composition (at.%): 7.03 Sm, 1.35 Zr, 66.16 Fe, 15.33 Co, 5.90 Ti, 4.23 O. The percentage of Sm (7.34, if only the metals are counted) is nominally sufficient to fill 95% of the 2*a* sites in the 1:12 structure. There exists, however, uncertainty with location of the oxygen atoms: whether they are in an undetected Sm oxide phase, in other oxide phases or even in the carbon tape used to secure the powder sample. The assumption that part of Sm is present as the oxide phase, whereas the other metal atoms are all in the 1:12 phase yields a formula $Sm_{0.815}Zr_{0.185}(Fe_{0.81}Co_{0.19})_{11.19}Ti_{0.81}$, which is reasonably close to the target composition. However, the hypothetical possibility that the detected oxygen is not part of the sample and that all Sm atoms are in the 1:12 structure would "place" most of the Zr atoms in the 8*i* sites – yielding a formula $Sm_{0.95}(Fe_{0.81}Co_{0.19})_{11.02}Ti_{0.80}Zr_{0.18}$. Situation of the Zr atoms in the 8*i* sites is contrary to the direct observations by Kobayashi at al. [20]. On the other hand, according to Matsumoto et al. [21], the respective formation energies should make the Zr atoms equally likely to occupy the 2*a* and 8*i* sites. It is thus conceivable that the Zr atoms site preference depends on the synthesis conditions. We attempted to refine the XRD data for $T_a = 1090$°C assuming the Zr atoms to be either in the 2*a* sites or in the 8*i* sites (see Supplementary material); the latter model was found to yield a slightly better ratio of the weighted-profile *R*-factor to the expected *R*-factor, 2.71 as compared to 3.86. Based on the above, the exact composition of the synthesized 1:12 compound and the sites preferences of the Zr atoms need to be clarified through additional studies.

Demagnetization curves of the alloys processed at 990–1220°C are shown in Fig. 2a. Difference between the curves measured parallel and perpendicular to the alignment (for clarity reasons, only three of the latter curves are shown) increases with the T_a – clearly indicating a continuing increase of magnetic anisotropy of the particles. The improved alignment leads to a nearly 50% increase of the remanent magnetization σ_r, from 84 to 124 A·m^2/kg. Even more remarkable is a simultaneous increase of the $\mu_0 H_c$ from 0.45 to 1.26 T. The latter $\mu_0 H_c$ value matches the one recently attained – through nanostructuring – in an epitaxially grown $Sm(Fe_{0.8}Co_{0.2})_{12}B_{0.5}$ thin film [22] and it represents a very significant progress for the *bulk* $Sm(Fe,Co,Ti)_{12}$ materials. As a downside, one has to note a poor "rectangularity" of the corresponding $\sigma(\mu_0 H)$ curve; this practically important characteristic appears to progressively degrade for the $T_a > 1090$°C. Consequently, the maximum energy product $(BH)_{max}$ of a hypothetical fully dense magnet corresponding to the powder processed at 1220°C is smaller than what is allowed by the σ_r value. The XRD data combined with the structural model in which the Zr atoms replace the Sm atoms in the 2*a* sites suggest a density of 7.72 g/cm^3; a $(BH)_{max}$ corresponding to this density is equal to 209 kJ/m^3 (26.3 MGOe) [if the Zr atoms occupied the 8*i* sites, the calculated density and $(BH)_{max}$ would be 7.89 g/cm^3 and 216.5 kJ/m^3 (27.2 MGOe), respectively]. It is worth noting that until now the highest calculated $(BH)_{max}$ reported for the 1:12 powders was 175 kJ/m^3 of the *metastable* $Nd(Fe,Mo)_{12}N$ powder [23]. When the T_a is increased to 1250°C, the alignment of magnetic crystallites in the alloy powder almost disappears, and the $\mu_0 H_c$ collapses to ≈0.1 T (Fig. 2b). The complex effect of the reduction-diffusion temperature on the $\mu_0 H_c$ is shown in Fig. 2c; it is consistent with the notion of a single-phase 1:12 region inferred from the XRD data.

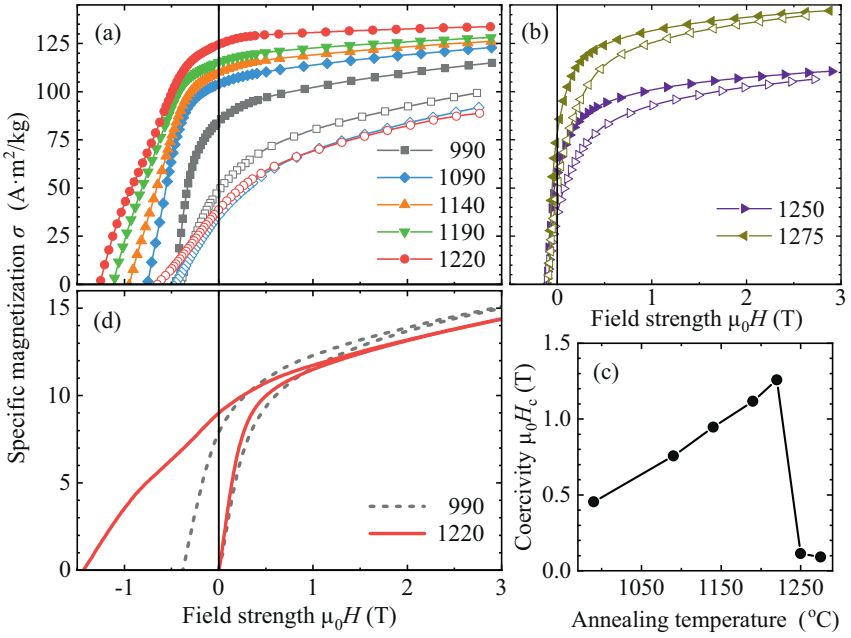

Fig. 2. Magnetic characterization of Sm–Zr–Fe–Co–Ti powders: (a and b) demagnetization curves of powders washed and field-oriented after reduction-diffusion synthesis at the indicated T_a (in °C); measurements *perpendicular* to the orienting field are shown with open symbols; (c) intrinsic coercivity measured parallel to the orienting field as a function of the T_a; (d) initial magnetization followed by pulse magnetizing and demagnetization for selected as-annealed (not washed, not oriented) powders. Data shown in part (d) were not corrected for the self-demagnetization.

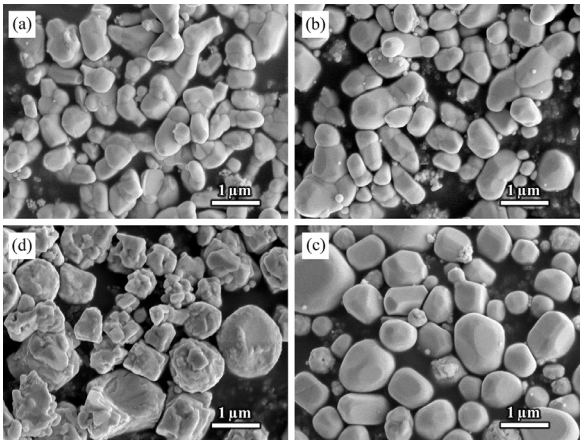

Fig. 3. SEM micrographs of Sm–Zr–Fe–Co–Ti powders washed after reduction-diffusion synthesis at different T_a: (a) 990°C, (b) 1090°C, (c) 1220°C, and (d) 1250°C

Table 1
Mean values of particle length L, particle width W, crystallite size D and volume-weighted crystallite size determined for Sm–Zr–Fe–Co–Ti powders synthesized at selected T_a.

T_a (°C)	Particle size		Crystallite size	
	$<L>$ (μm)	$<W>$ (μm)	$<D>$ (μm)	$(<D^3>)^{1/3}$ (μm)
990	1.06	0.50	0.26	0.35
1090	0.64	0.41	0.25	0.40
1220	0.65	0.53	0.34	0.54

Representative secondary-electrons SEM images of the powders processed at four selected T_a are shown in Fig. 3. Mean values of characteristic dimensions for the powders exhibiting high $\mu_0 H_c$ are listed in Table 1 (see also Supplementary material). Because the distributions of crystallite sizes D were found to be broad, the *volume-weighted* mean sizes $(<D^3>)^{1/3}$ must represent contributions of the crystallites to the sample magnetization more accurately than mean sizes $<D>$. The particle synthesized at 990°C is typically made of a chain of several crystallites and it has a mean aspect ratio of 2.1. When the T_a is increased to 1090°C, the crystallite size increases from 0.35 to 0.40 μm and the particle aspect ratio decreases; the particles now incorporate fewer crystallites and more particles appear monocrystalline. When the T_a is further increased to 1220°C, the crystallite size increases to 0.54 μm with almost all particles found to be monocrystalline and equiaxed (the mean aspect ratio 1.2). This evolution of the particle structure readily explains the effect of T_a on the degree of magnetic-field-induced texture. Because within polycrystalline particles the [001] easy magnetization directions vary from crystallite to crystallite, only the monocrystalline particles can be perfectly oriented by the aligning magnetic field (see Fig. 4). The reasons for the simultaneous increase of the $\mu_0 H_c$ are less obvious, but in addition to elimination of the grain boundaries leading to a better magnetic insulation of the crystallites, they probably include reduced incidence of lattice defects, such as the twin boundaries. It is remarkable that in this experiment, the $\mu_0 H_c$ and the crystallite size increase simultaneously. This may seem contrary to the usually observed trend, unless such trend – often explained via the critical single-domain particle or crystallite size – actually reflects incidence of the lattice defects [24]. The initial magnetization curves of the powders synthesized at 990 and 1220°C (measured *before* the washing, as the latter exposed the material to a magnetic field), which are shown in Fig. 2d, are both characterized by a high initial susceptibility.

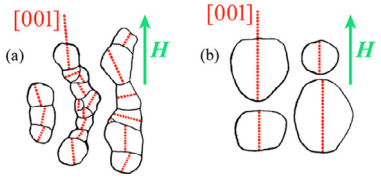

Fig. 4. Schematic representation of magnetic-field-induced alignment of the [001] easy magnetization directions in the 1:12 crystallites synthesized at (a) 990°C and (b) 1220°C.

This indicates that no single domain 1:12 crystallites are present in the thermally demagnetized powders, and that magnetization reversal in the powders synthesized at any T_a is controlled by nucleation of magnetic domain walls.

The particles synthesized at 1250°C appear in the SEM image (Fig. 3d) as neither monocrystalline, nor incorporating only a few crystallites. Their obvious polycrystallinity explains the low degree of texture induced by the magnetic-field alignment. Their low $\mu_0 H_c$, on the other hand, must be due to presence of the soft-magnetic bcc and semihard 1:7 phases, and possibly also due to an inadequate magnetic insulation of the 1:12 crystallites. The ongoing investigation of the effects of specific elements on the results of the high-temperature reduction-diffusion synthesis is expected to explain why this processing did not develop a high $\mu_0 H_c$ in the alloy with nominal composition $Sm_{0.9}Zr_{0.1}(Fe_{0.75}Co_{0.25})_{11.35}Ti_{0.65}$ [18]. Our preliminary data point at a strong influence of the Zr content as a possible reason.

In conclusion, we have discovered that reduction-diffusion treatment done just below the upper boundary of the 1:12 phase temperature range can overcome the factors (supposedly associated with structural defects) which hold back the coercivity of the traditionally prepared $Sm(Fe,Co,Ti)_{12}$ alloys. The magnetically anisotropic powders prepared through this process may be considered promising precursors for the development of bonded and sintered 1:12 permanent magnets.

Acknowledgements

This work was supported by the U.S. Department of Energy [grant number DE-FG02-90ER45413]. The authors are grateful to Chaoya Han and Dr. Chaoying Ni of the University of Delaware W.M. Keck Center for Advanced Microscopy and Microanalysis for the EDS characterization.

Declaration of Competing Interest

The authors declare that they have no known competing financial interests or personal relationships that could have appeared to influence the work reported in this paper.

Supplementary materials

Supplementary material associated with this article can be found, in the online version, at doi:10.1016/j.scriptamat.2021.113760.

References

[1] T. Kuno, S. Suzuki, K. Urushibata, K. Kobayashi, N. Sakuma, M. Yano, A. Kato, A. Manabe, AIP Adv. 6 (2016) 025221.
[2] P. Tozman, H. Sepehri-Amin, Y.K. Takahashi, S. Hirosawa, K. Hono, Acta Mater. 153 (2018) 354.
[3] M. Hagiwara, N. Sanada, S. Sakurada, J. Magn. Magn. Mater. 465 (2018) 554.
[4] A.M. Schönhöbel, R. Madugundo, J.M. Barandiarán, G.C. Hadjipanayis, D. Palanisamy, T. Schwarz, B. Gault, D. Raabe, K. Skokov, O. Gutfleisch, J. Fischbacher, T. Schrefl, Acta Mater. 200 (2020) 652.
[5] T. Kuno, S. Suzuki, K. Urushibata, K. Kobayashi, S. Sugimoto, Mater. Trans. 60 (2019) 1697.
[6] I. Dirba, J. Li, H. Sepehri-Amin, T. Ohkubo, T. Schrefl, K. Hono, J. Alloys Compd. 804 (2019) 155.
[7] I. Dirba, H. Sepehri-Amin, T. Ohkubo, K. Hono, Acta Mater. 165 (2019) 373.
[8] I. Dirba, H. Sepehri-Amin, I.-J. Choi, J.-H. Choi, H.-S. Uh, T.-H. Kim, S.-J. Kwon, T. Ohkubo, K. Hono, J Alloys Compd. (2020), doi:10.1016/j.jallcom.2020.157993.
[9] J. Ding, M. Rosenberg, J. Less-Common Met. 161 (1990) 263.
[10] J. Wecker, M. Katter, K. Schnitzke, L. Schultz, J. Appl. Phys. 67 (1990) 4951.
[11] S. Sugimoto, A. Kojima, M. Okada, M. Homma, Mater. Trans. 32 (1991) 1180.
[12] T. Kuno, T. Yamamoto, K. Urushibata, K. Kobayashi, S. Sugimoto, Mater. Trans. 61 (2020) 657.
[13] D. Palanisamy, S. Ener, F. Maccari, L. Schäfer, K.P. Skokov, O. Gutfleisch, D. Raabe, B. Gault, Phys. Rev. Mater. 4 (2020) 054404.
[14] F. Maccari, L. Schäfer, I. Radulov, L.V.B. Diop, S. Ener, E. Bruder, K. Skokov, O. Gutfleisch, Acta Mater. 180 (2019) 15.
[15] A.M. Gabay, A. Martín-Cid, J.M. Barandiaran, D. Salazar, G.C. Hadjipanayis, AIP Adv. 6 (2016) 056015.
[16] Q.M. Cheng, J.H. Lin, M.Z. Su, J. Alloys Compd. 280 (1998) 310.
[17] A.M. Gabay, G.C. Hadjipanayis, J. Magn. Magn. Mater. 422 (2017) 43.
[18] G.C. Hadjipanayis, A.M. Gabay, A.M. Schönhöbel, A. Martín-Cid, J.M. Barandiaran, D. Niarchos, Eng. J. 6 (2020) 141.
[19] W. Kraus, G. Nolze, J. Appl. Crystallogr. 29 (1996) 301.
[20] K. Kobayashi, S. Suzuki, T. Kuno, K. Urushibata, N. Sakuma, M. Yano, T. Shouji, A. Kato, A. Manabe, J. Alloys Compd. 694 (2017) 914.
[21] M. Matsumoto, T. Hawai, K. Ono, Phys. Rev. Appl. 13 (2020) 064028.
[22] H. Sepehri-Amin, Y. Tamazawa, M. Kambayashi, G. Saito, Y.K. Takahashi, D. Ogawa, T. Ohkubo, S. Hirosawa, M. Doi, T. Shima, K. Hono, Acta Mater. 194 (2020) 337.
[23] Y. Yang, J. Yang, J. Han, C. Wang, S. Liu, H. Du, IEEE Trans. Magn. 52 (2015) 2103806.
[24] K. Kobayashi, R. Skomski, J.M.D. Coey, J. Alloys Compd. 222 (1995) 1.